Volume 10
Number 11
21 March 2022
Pages 1677–1888

Journal of Materials Chemistry B

Materials for biology and medicine

rsc.li/materials-b

ISSN 2050-750X

ROYAL SOCIETY OF CHEMISTRY

PAPER

Jie Zheng *et al.*

Conformational-specific self-assembled peptides as dual-mode, multi-target inhibitors and detectors for different amyloid proteins

Journal of Materials Chemistry B

ROYAL SOCIETY OF CHEMISTRY

PAPER

View Article Online
View Journal | View Issue

Cite this: J. Mater. Chem. B, 2022, 10, 1754

Conformational-specific self-assembled peptides as dual-mode, multi-target inhibitors and detectors for different amyloid proteins†

Baiping Ren,‡ Yijing Tang,‡ Dong Zhang, Yonglan Liu, Yanxian Zhang, Hong Chen, Rundong Hu, Mingzhen Zhang and Jie Zheng *

Received 17th December 2021,
Accepted 31st January 2022

DOI: 10.1039/d1tb02775a

rsc.li/materials-b

Prevention and detection of misfolded amyloid proteins and their β-structure-rich aggregates are the two promising but different (pre)clinical strategies to treat and diagnose neurodegenerative diseases including Alzheimer's diseases (AD) and type II diabetes (T2D). Conventional strategies prevent the design of new pharmaceutical molecules with both amyloid inhibition and detection functions. Here, we propose a "like-interacts-like" design principle to *de novo* design a series of new self-assembling peptides (SAPs), enabling them to specifically and strongly interact with conformationally similar β-sheet motifs of Aβ (association with AD) and hIAPP (association with T2D). Collective *in vitro* experimental data from thioflavin (ThT), atomic force microscopy (AFM), circular dichroism (CD), and cell assay demonstrate that SAPs possess two integrated functions of (i) amyloid inhibition for preventing both Aβ and hIAPP aggregation by 34–61% and reducing their induced cytotoxicity by 7.6–35.4% and (ii) amyloid sensing for early detection of toxic Aβ and hIAPP aggregates using in-house SAP-based paper sensors and SPR sensors. The presence of both amyloid inhibition and detection in SAPs stems from strong molecular interactions between amyloid aggregates and SAPs, thus providing a new multi-target model for expanding the new therapeutic potentials of SAPs and other designs with built-in amyloid inhibition and detection functions.

1. Introduction

Aggregation of misfolded amyloid proteins, which differ widely in sequence, size, native structure, and biological function, into β-sheet-rich aggregates is a common pathological hallmark of many protein misfolding diseases (PMDs) such as Alzheimer's disease (AD) and type II diabetes (T2D).[1] β-sheet-rich amyloid aggregates are regarded as ideal biomarkers for developing new molecular ligands for therapeutic prevention and disease diagnosis. While amyloid-binding ligands have been extensively studied and developed, they are mostly limited to a single target against a specific amyloid protein or a single function as amyloid inhibitors or amyloid probes, thus leading to marginal benefits of these amyloid-binding ligands for amyloid detection, medical treatments, and disease diagnosis.[2] It is highly important, but a great challenge, to develop multi-functional and multi-target molecular ligands for achieving both early detection and prevention of different amyloid aggregates, which are the keys to understanding and defeating PMDs.

Amyloid detectors and amyloid inhibitors, despite differences in their biological functions and practical uses, share a similar working principle to achieve their respective functions *via* specific recognition and strong interaction with amyloid proteins. However, almost all amyloid-binding ligands still possess either property, *i.e.*, amyloid detectors do not function as amyloid inhibitors, and *vice versa*. Different from conventional amyloid-binding ligands (*e.g.*, antibodies,[3,4] polymers,[5,6] nanoparticles,[7–9] organic molecules,[10,11] and drugs[12,13]), small peptides,[14–17] despite being less explored, are developed as highly sensitive and specific binding molecules for either inhibiting or detecting amyloid proteins, due to several intrinsic advantages of small sizes for mass production at low cost, ease of sequence/structural modifications to realize high bioactivity, and less susceptibility to proteolytic degradation. However, challenges still largely remain for developing peptide-based amyloid inhibitors or detectors. First, these amyloid-binding peptides are mostly workable for specific amyloid proteins, showing highly sequence-dependent binding behavior, which prohibits amyloid-binding peptides to be used as general recognition molecules for different amyloid proteins. Second, conventional design strategies

Department of Chemical and Biomolecular Engineering, The University of Akron, Akron, Ohio 44325, USA. E-mail: zhengj@uakron.edu

† Electronic supplementary information (ESI) available. See DOI: 10.1039/d1tb02775a

‡ These authors contributed equally to this work.

of amyloid-binding peptides mainly aim to use amyloid fragments derived from their parent amyloid proteins as recognition agents to bind to their parent amyloid proteins for either detecting or inhibiting amyloid aggregation. For example, $A\beta_{31-42}$, $A\beta_{39-42}$, $A\beta_{16-20}$, $A\beta_{17-21}$,[18–22] and their analogues[23] demonstrated their inhibitory ability to prevent Aβ formation, while $hIAPP_{20-25}$ and $hIAPP_{24-29}$ were identified as amyloid inhibitors to prevent full-length $hIAPP_{1-37}$ aggregation and fibrillization.[24,25] Since these amyloid fragmental peptides are mainly derived from their parent proteins, it is not surprising that they can bind to the homologous sequences of the corresponding amyloid proteins and can interfere with the aggregation of their parent amyloid proteins, but not other amyloid proteins.[26,27] It is also disappointing that none of these Aβ or hIAPP fragments have been used as recognition ligands in biosensors/bioassays for the detection of Aβ or hIAPP aggregates. Third, an additional obstacle is that amyloid-derived peptides have inherent disadvantages, such as very limited sequence diversity, poor proteolytic degradation, and low anti-amyloid activity. Therefore, it is imperative to *de novo* design new amyloid-binding peptides, not derived from amyloid sequences, for inhibiting and detecting different amyloid proteins.

Motivated by these challenges, we proposed a structural-based *de novo* design of a family of conformation-sensitive, sequence-independent, multi-target, self-assembling peptides (SAPs),[28] which possess a dual built-in function as (i) amyloid inhibitors to prevent the aggregation of both Aβ (associated with AD) and hIAPP (associated with T2D) in solution and (ii) surface-immobilized amyloid detectors to sense both Aβ and hIAPP aggregates. Our working hypothesis of SAPs as both amyloid inhibitors and detectors is built on the facts that since all amyloid aggregates possess the common β-sheet structures, in principle we can design some conformational-specific peptides that can fold into a β-sheet-rich structure, which would serve as a general binding motif to specifically interact with a similar β-sheet structure of amyloid aggregates in a sequence-dependent manner. Secondly, since both ''inhibition'' and ''detection'' of amyloid aggregates by such β-sheet-specific peptides are essentially governed by a similar/same working principle (*i.e.*, by homotypic, specific, and sequence-independent β-sheet interactions between peptides and amyloids), the β-sheet-specific peptides could also function as amyloid detectors and amyloid inhibitors for different amyloid proteins. As a result, our SAPs demonstrated not only their self-assembling ability to form β-sheet-rich fibrils, but also the strong inhibition ability to prevent the aggregation and cell toxicity of both Aβ and hIAPP. Further structural studies confirm that this general inhibition ability of SAPs against both Aβ and hIAPP aggregation mainly stems from the specific β-sheet interactions between SAPs and amyloid aggregates. More importantly, such strong β-sheet interactions between SAPs and amyloid proteins enabled SAPs to possess a detection ability for Aβ and hIAPP proteins. Evidently, we developed two prototype sensors (a paper sensor and a SPR sensor) by anchoring SAPs on different substrates, and both SAP sensors were able to detect both Aβ and hIAPP aggregates. To date, the vast majority of current studies have been mostly limited to develop antibody-based, fluorescence-based, nanoparticle-based, and aptamer-based amyloid probes/sensors,[2,29] however, peptide-based amyloid probes and sensors are still very scarce.[30] All of these amyloid probes/sensors either only possess a single recognition ability to detect amyloid aggregates or single-target probes that only target a specific amyloid protein. To our knowledge, we are the first to develop multiple-mode and multi-target amyloid probes for the early and enhanced detection of multiple pathological aggregates and co-aggregates formed by different amyloid proteins (Aβ associated with AD and hIAPP associated with T2D), and demonstrate that (i) the SAPs offer a conformational-specific biorecognition mechanism to selectively interact with unique β-sheet motifs of amyloid aggregates in a sequence-independent manner and (ii) the SAPs serve as generic amyloid inhibitors to prevent both Aβ and hIAPP aggregation/toxicity, as well as generic peptide-based biosensors to detect different Aβ and hIAPP aggregates in a sequence-independent manner.

2. Experimental

2.1 Reagents and instruments

All reagents and related instruments used in the experiments are listed in the ESI.†

2.2 Paper sensor preparation

Hexapeptides with the sequence of CILFWG, CTIYWG, CTLWWG, GTVWWG, IQIMIW, VTLWWG, CTVWWG, CTVFIG, VYIMIG, ITLFWG, GTLFWG, PTRCGP, $A\beta_{27-32}$ and $hIAPP_{1-6}$ were synthesized on an amino-modified acid stable cellulose membrane with a PEG-spacer (AIMS Scientific Product) as described (Frank *et al.*, 1992). After synthesis, the membranes were blocked with 2% skim milk powder in TBS-T (0.01% Tween 20) overnight at 4 °C, followed by incubating with biotinylated Aβ or hIAPP at room temperature for 6 h. The membrane was washed with TBS-T three times. Membrane bound biotinylated Aβ or hIAPP were detected following incubation with streptavidin–POD for 90 min at room temperature and then incubated with supersignal west Dura Chemiluminescence Reagent.

2.3 Synthesis of 3D carboxymethyl dextran SPR chips

The 3D carboxymethyl dextran sensor chip was first fabricated. The gold sensor chip surfaces were cleaned by rinsing in ethanol and water sequentially, treating under UV/ozone for 20 min, followed by immersion in a 1 : 1 : 5 (v/v/v) solution of H2O2 (30%), NH3 (25%), and ultrapure water for 15 min at 85 °C. After thoroughly rinsing with ultrapure water the chips were ultra-sonicated in 99.5% ethanol for 10 min, and then dried under a nitrogen flow. The cleaned chips were then immersed in a 1 mM solution of HS–$(CH2)_{16}$–OH in 99.5% ethanol at room temperature for 16 h and were washed with ethanol and ultrapure water. The chips were then reacted with 0.6 M epichlorohydrin dissolved in a 1 : 1 mixture of diglyme and 0.4 M sodium hydroxide on a shaking-table for 4 h at room temperature. After washing with water, the chips were immersed in a dextran solution (5 g dextran 500 kDa, in

25 mL 0.4 M sodium hydroxide) and incubated on a shaking-table for 26 h at room temperature. Further carboxylation was done by reaction with 1 M bromoacetic acid in 2 M sodium hydroxide at room temperature for 16 h. Finally, the chips were washed with ultrapure water three times and stored in nitrogen at 0–8 °C.

2.4 SAP-coated SPR sensor

A custom-built four-channel SPR sensor based on wavelength interrogation was used to perform the real-time monitoring of amyloid peptide (Aβ or hIAPP) absorption on hexapeptides. A CBD-modified SPR sensor chip was prepared based on a well-established method (Löfås *et al.*,1990). Briefly, the gold surfaces were completely cleaned by using acetone, Milli-Q, and alcohol before immersing in 5 mM 11-mercapto-1-undecanol in ethanol/water (8 : 2) solution for 24 h. Subsequently, these surfaces were reacted with epichlorohydrin (2% v/v) in 0.1 M NaOH for 3 h and transferred to 6 kDa dextran solution in 0.1 M NaOH for 24 h. Finally, they were immersed in 1 M bromoacetic acid in 2 M NaOH for another 24 h and dried with an air stream to obtain the CBD-modified SPR chips. For hexapeptide immobilization, the PBS buffer was first injected to flow through four separated channels under the pressure of a peristaltic pump for 10 min to get a stable baseline. Then, the CBD-modified SPR chips were activated by using an equimolar mix of EDC(*N*-ethyl-*N*-(diethyl-aminopropyl) carbodiimide) and NHS (*N*-hydroxysuccinimide), followed by quickly washing with PBS buffer. Then, hexapeptide dissolved in sodium acetate (10 mM, pH = 5.2) was introduced onto the sample surface for 10 min, and the remaining NHS–ester groups were blocked by a flow of 1 M ethanolamine HCL for another 10 min. The interaction of hexapeptide with Aβ or hIAPP was performed by injecting a serial dilution of Aβ or hIAPP (0.05–0.1 mg mL^{-1}) in running buffer (10 mM PBS, pH 7.4) over channels at a flow rate of 10 μL min^{-1}, followed by PBS buffer to remove any unbound Aβ or hIAPP. Aβ/hIAPP absorption was quantified by measuring the wavelength changes before and after the absorption. In this work, 1 nm of the SPR wavelength shift at 750 nm represents a surface coverage of ~15 ng cm^{-2} protein absorption. An SPR experiment under each condition was repeated twice.

3. Results and discussion

3.1 SAPs exhibit a self-assembling capacity

In our previous studies,[28,31] we developed a data-driven computational platform – combining molecular docking, molecular dynamics (MD) simulation, and a QSAR (quantitative structure–activity relationship) model – for the high-throughput screening and design of six-residue SAPs that can computationally fold into β-sheet structures similar to the cross-β-sheet in amyloid fibrils. To experimentally confirm our computational designs, we selected six hexapeptides of CILFWG (**HP1**), CTLWWG (**HP2**), CTIYWG (**HP3**), VYIMIG (**HP4**), CTVFIG (**HP5**), and GTVWWG (**HP6**) to examine their capacity for the formation of β-sheet structures in amyloid-like fibrils. As shown in Fig. 1a, six

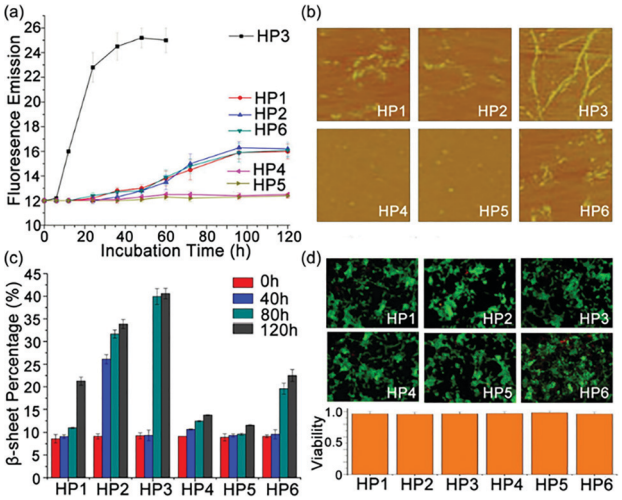

Fig. 1 Structural and biocompatibility characterizations of six SAPs (100 μM) of CILFWG (**HP1**), CTLWWG (**HP2**), CTIYWG (**HP3**), VYIMIG (**HP4**), CTVFIG (**HP5**), and GTVWWG (**HP6**) by (a) aggregation kinetics using a ThT fluorescence assay, (b) aggregation morphologies using AFM images, (c) structural transition using CD spectroscopy, (d) cell viability using SH-SY5Y cells in MTT and cell live/dead assays. All error bars represent the average of three–five replicate experiments.

hexapeptides (100 μM) incubated at 37 °C exhibited three different aggregation kinetics. **HP3** exhibited a strong self-assembling ability to form amyloid-like β-structures, as evidenced by typical amyloid-like aggregation kinetics, starting with a short lag phase of 6 h, followed by a sharp growth phase between 6–45 h, and eventually achieving an equilibrium phase with a maximum ThT fluorescence intensity of ~25. The AFM images (1 × 1 μm) in Fig. 1b also confirmed that **HP3** formed thin, long, and ribbon-like fibrils with fibril heights of 2–4.5 nm and fibril lengths of 300–800 nm. CD spectra also show that as the incubation time proceeded, **HP3** underwent structural transition from random coils to β-sheets (Fig. S1, ESI†) and increased its β-sheet component from 9.28% at 0 h to 40.59% at 120 h (Fig. 1c). **HP1**, **HP2**, and **HP6** exhibited a moderate self-assembling ability to form β-sheet-rich structures and amyloid-like aggregates. Evidently, the three SAPs showed almost identical aggregation kinetics curves with the longer lag phase (12–24 h), the slower growth phase (12–96 h), and the relatively lower equilibrium phase (Fig. 1a), leading to many short worm-like filaments of 0.5–2.0 nm in height and 100 nm in length (Fig. 1b). The three SAPs also experienced a similar structural transition towards β-sheet structures by a slowly emerging broad minimum at ~217 nm and a disappeared negative peak at 197 nm, resulting in the final β-sheet contents of **HP1**, **HP2**, and **HP6** being 21.27%, 33.86% and 22.5%, respectively (Fig. 1c), indicating that less β-sheet fibrils are produced as compared to **HP3**, again consistent with the ThT and AFM data. In sharp contrast to the four SAPs above, **HP4** and **HP5** almost did not form observable amyloid-like fibrils instead of several dispersed spherical particles with diameters of ~1 nm (Fig. 1b), with much fewer β-structures of 11.58–13.76% (Fig. 1a and c). Collective ThT, AFM, and CD results demonstrated that among these SAPs, **HP3**, **HP1**, **HP2**, and **HP6**

were capable of self-assembling into β-sheet structures to different extents, of which **HP3** exhibits a better β-sheet-forming property than the others. Sequence comparison appears to suggest that tyrosine in **HP3** with additional phenolic hydroxyl facilitates the formation of a β-sheet structure *via* hydrogen bonding. We also tested the cell toxicity of the six SAPs using both MTT and live/dead cell assays with the SH-SY5Y cell line. The MTT results in Fig. 1d show that after incubating each SAP (100 μM) with cells for 120 h, all SAPs presented almost no cytotoxicity to cells, as evidenced by >97% cell viability relative to the control without peptide addition. Cell live/dead images further showed that dominantly living cells exhibited rich synapses (*i.e.*, differentiated state). Particularly those SAPs adopting β-sheet structures did not possess peptide-induced cell toxicity.

3.2 SAPs modulate the aggregation and fibrillization of both Aβ and hIAPP

Upon demonstrating that SAPs possess a self-assembling ability to fold into common β-sheet-rich structures similar to amyloid proteins (not limited to Aβ and hIAPP), next we propose the "like-interacts-like" mechanism, *i.e.*, β-structure-forming SAPs are expected to interact strongly with conformationally similar β-structure-rich amyloid aggregates, which will in turn competitively reduce amyloid–amyloid interactions and prevent amyloid aggregation. To test this hypothesis, we first examined the inhibition effects of six SAPs on the aggregation of both Aβ and hIAPP using ThT spectroscopy. Each SAP was separately incubated with freshly prepared Aβ or hIAPP solution (25 μM) at three different amyloid:SAP ratios (1 : 2, 1 : 4, and 1 : 6) at 37 °C for 24 h. As shown in the control groups (Fig. 2a1 and b1), pure Aβ or pure hIAPP (25 μM) alone gave rise to typical nucleation-polymerization aggregation profiles, starting with a lag phase of ~4–5 h, followed by a rapid growth phase of 5–15 h, and ending at a stable ThT plateau of ~170 and 53 after 15 h, respectively. Upon incubation of SAPs with Aβ or hIAPP, six ThT aggregation profiles can be classified into three groups: inhibition (**HP1**, **HP2**, **HP6**), no-effect (**HP4**, **HP5**), and promotion (**HP3**) groups. Evidently, **HP1**, **HP2**, and **HP6** imposed strong concentration-dependent inhibition effects on both Aβ and hIAPP aggregation as indicated by the significant decrease in fluorescence intensity. Namely, as compared to the pure Aβ or hIAPP without SAPs, **HP1**, **HP2**, and **HP6** largely reduced the final fluorescence intensity of the Aβ fibrils by 34–45%, 30–40%, and 36–43% and of hIAPP fibrils by 38–61%, 42–60%, and 35–56%, respectively, at three amyloid:SAP ratios. This amyloid inhibition effect not only increased with SAP concentration, but also occurred at three aggregation phases along the Aβ or hIAPP aggregation pathways, during which the SAPs prolonged their lag phase by 4–6 h, decreased the aggregation rates at the growth phase, and reduced the final fibrillization at the equilibrium phase. Furthermore, the inhibition activity of the three SAPs to inhibit Aβ or hIAPP fibril formation was also confirmed by AFM images (Fig. 2a2 and b2).

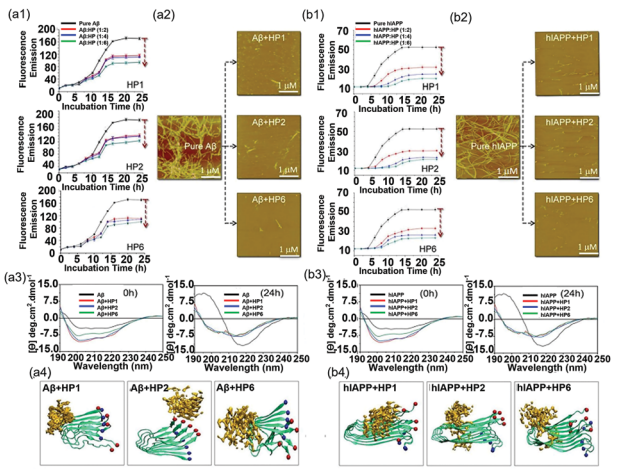

Fig. 2 Dual inhibition effects of CILFWG (**HP1**), CTLWWG (**HP2**), and GTVWWG (**HP6**) on both Aβ and hIAPP aggregations. (a1, b1) Time-dependent ThT fluorescence curves and (a2, b2) AFM images (scale bar = 1 μm) at different molar ratios of amyloid : SAP = 1 : 2, 1 : 4, and 1 : 6, (a3, b3) CD spectrum at amyloid : SAP molar ratio = 1 : 6, and (a4, b4) hotspot bindings of Aβ and hIAPP in the presence of **HP1**, **HP2**, and **HP6**.

Molecular dynamics (MD) simulations further revealed preferential binding positions of different SAPs around Aβ or hIAPP aggregates. Analysis of the contact probability between SAPs and Aβ or hIAPP aggregates clearly indicated that the SAPs preferentially interacted with the β-sheet groove and turn regions, two signature motifs in both Aβ or hIAPP aggregates, where most of the hydrophobic residues (*e.g.* Gly, Phe, Leu of Aβ and Phe, IIe, Leu of hIAPP) were located in these two regions. This strong binding of SAPs to these two regions not only disturbed the conformations of Aβ or hIAPP aggregation, but also prevented amyloid growth *via* either monomer attachment for elongation or lateral stacking. Thus, MD simulations confirm that the greater common inhibition of SAPs stems from strong interaction with amyloid proteins to prevent amyloid–amyloid interactions from their self-aggregations (Fig. 2a4, b4 and Fig. S2, ESI†).

Of note, **HP3** that possesses the strongest self-assembling ability to form a β-sheet structure exhibited a contrasting role

in the aggregation of Aβ and hIAPP. ThT data in Fig. S3 (ESI†) showed that **HP3** at all tested concentrations significantly reduced Aβ fibrillization by 31.6–48.0% but promoted hIAPP fibrilization by 9.3–27.8%. In the case of the **HP3**–hIAPP system, **HP3** initially inhibited the early nuclei formation of hIAPP by lengthening its lag phase by 2–4 h, but once hIAPP seeds were formed, they recruit both hIAPP and **HP3** to form more hybrid fibrils, thus promoting hIAPP fibrillation ultimately. AFM images also supported this observation that the presence of **HP3** promoted hIAPP fibril formation, in sharp contrast to the significant reduction in Aβ fibrils (Fig. S4, ESI†). CD data consistently showed that co-incubation of **HP3** with Aβ decreased the final β-structure content to 40%, as compared to the 49% β-structure for pure Aβ, but hIAPP with and without **HP3** showed a similar β-structure content of 40% *vs.* 41% (Fig. S5, ESI†). For **HP4** and **HP5**, the incubation of either SAPs with Aβ or hIAPP at different molar ratios yielded almost the same ThT aggregation curves as those formed by pure Aβ or pure hIAPP. Little or no change in the ThT fluorescence intensity clearly indicates that **HP4** and **HP5** have no or little influence on Aβ or hIAPP aggregation (Fig. S3, ESI†). The AFM images in Fig. S4 (ESI†) consistently showed that the presence of **HP4** and **HP5** in Aβ or hIAPP solution still produced long and densely branched fibrils with the height of 4–12 nm and the length of 1–2.5 μm, whose morphologies and sizes were similar to those of Aβ or hIAPP fibrils alone. Both the ThT and AFM data indicate no or undetectable effect of **HP4** and **HP5** on Aβ or hIAPP aggregation. The different inhibitory activities by SAPs could be due to different specific folding enabling specific side-chain topologies and high-affinity functional interactions with Aβ or hIAPP.

3.3 SAPs alleviate both Aβ- and hIAPP-induced cytotoxicity

Upon demonstrating the inhibitory activity of the three SAPs (**HP1**, **HP2**, and **HP6**) against amyloid aggregation, we next examined whether these three SAPs could also protect cells from both Aβ- and hIAPP-induced cell toxicity. Human neuroblastoma cells (SH-SY5Y, Aβ) or rat insulinoma cells (RIN-m5F cells, hIAPP) in MTT and live/dead cell assays were used and incubated with Aβ (25 μM) or hIAPP (25 μM) alone or with SAPs (50, 100 and 150 μM) at 37 °C for 24 h. In Fig. 3a, as a control, pure Aβ (25 μM) and pure hIAPP (25 μM) caused 54.5% and 42.3% death of SH-SY5Y and RIN-m5F cells, respectively. When introducing three different SAPs of different concentrations (50, 100, and 150 μM) into Aβ- or hIAPP-containing (25 μM) cell cultures, **HP1**, **HP2**, and **HP6** exhibited a protecting role in rescuing cells from Aβ- and hIAPP-induced cell toxicity at all three concentrations, and the inhibitory activity of SAPs to suppress cell damage increased with the concentrations. At the highest SAP concentration of 150 μM, **HP1**, **HP2**, and **HP6** increased the viability of SH-SY5Y cells treated with Aβ to 62.5%, 83.1%, and 80.9%, as well as RIN-m5F cells treated with hIAPP to 86.5%, 84.8%, and 89.6%, respectively. Thus, **HP1**, **HP2**, and **HP6** can protect the cells from amyloid-induced toxicity by reducing their aggregations or forming no/less toxic SAP–amyloid complexes. Fig. 3b consistently shows that (i) Aβ and hIAPP alone exhibited high toxicity to cells, as observed by the large proportion of dead cells (red stains) as compared to live ones (green stains); (ii) co-incubation of **HP1**, **HP2**, and **HP6** with hIAPP led to much fewer dead cells as compared with the pure amyloid system, again confirming the protection ability of SAPs from amyloid-induced cell toxicity. Differently, **HP3** with a concentration of 150 μM suppressed Aβ-induced SH-SY5Y damage and thus increased its cell viability by 22.2% but showed little protection of RIN-m5F cells from hIAPP-induced toxicity as evidenced by a similar cell viability (59.2%) to the control group (57.7%) (Fig. S6, ESI†). In the cases of **HP4** and **HP5**, both SAPs were ineffective in reducing Aβ-induced SH-SY5Y and hIAPP-induced RIN-m5F toxicity, and the increase in concentration of both SAPs from 50 μM to 150 μM did not improve the cell viability as compared to pure Aβ- or hIAPP-treated control groups. Combining the inhibition of amyloid aggregation and toxicity by SAPs reveals the structure–toxicity correlation of SAPs, *i.e.*, the loss-of-toxicity activity of Aβ and hIAPP aggregates is directly linked to the reduction of their aggregates as inhibited by SAPs.

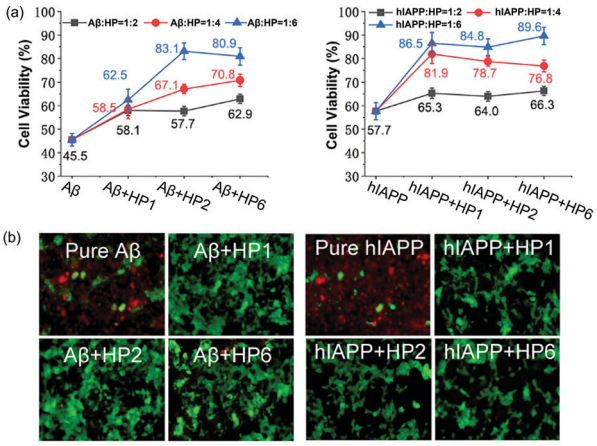

Fig. 3 Dual inhibition effects of CILFWG (**HP1**), CTLWWG (**HP2**), and GTVWWG (**HP6**) on the Aβ-induced SH-SY5Y and hIAPP-induced RIN-m5F toxicity using (a) an MTT assay at different amyloid (25 μM) : SAP (50, 100, and 150 μM) ratios and (b) a live/dead cell assay at a specific amyloid (25 μM):SAP (150 μM) ratio.

3.4 SAP-coated paper sensor to detect Aβ and hIAPP

Considering that both "inhibition" and "detection" of amyloid aggregates requires strong interactions to occur between SAPs and amyloids, we developed a cellulose paper sensor by synthesizing the SAPs onto a PEG-Spaced Cellulose Membrane. Fig. 4a illustrates a working principle of the SAP-coated paper sensors, *i.e.*, (i) a superhydrophilic poly(ethylene glycol) (PEG) spacer was used as a general antifouling background to resist nonspecific protein adsorption and to ensure low-noise detection signals, while anchored SAPs were used as detection agents to detect biotinylated Aβ and hIAPP (biotin–Aβ and biotin–hIAPP); (ii) the SAPs that can bind both biotin–Aβ and biotin–hIAPP will be used as general amyloid detection agents, because bound biotin–Aβ and biotin–hIAPP can further be specifically recognized by streptavidin-conjugated peroxidase (POD) to show the different extents of chemiluminescence.

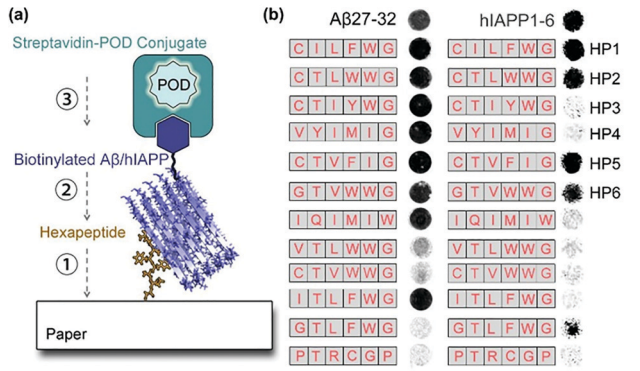

Fig. 4 (a) Schematic of SAP-immobilized cellulose paper sensors for amyloid detection; (b) Visual inspection of immobilized SAPs for detecting biotin–Aβ and biotin–hIAPP, where the SAP–biotin–Aβ/hIAPP complexes are further separated by native SDS–PAGE and visualized by streptavidin–POD.

As shown in Fig. 4b, **HP1**, **HP2**, and **HP6** showed a strong and specific binding affinity to both biotin–Aβ and biotin–hIAPP, and their binding affinities were comparable to those between $Aβ_{27–32}$ fragments and biotin–Aβ and between $hIAPP_{1–6}$ fragments and biotin–hIAPP (positive controls). **HP3** only recognized Aβ, not hIAPP. Of note, our previous data showed that **HP4** and **HP5** presented a lower self-assembling ability to form a β-sheet structure in solution and thus failed to prevent the aggregation and cytotoxicity of Aβ and hIAPP. However, the immobilized **HP5** were able to specifically recognize both biotin–Aβ and biotin–hIAPP, while the immobilized **HP4** only bound to biotin–Aβ. This was possibly because the surface immobilization of peptides (not limited to SAPs) will increase their surface packing density, which may promote the formation of the ordered secondary structures and thus increase the binding probability to amyloid peptides. We further studied the mutation effects of an additional six SAPs (IQIMIW, VTLWWG, CTVWWG, ITLFWG, GTLFWG, and PRTCGP) on the binding affinity of biotin–Aβ and biotin–hIAPP. Among them, VTLWWG, CTVWWG, and PRTCGP did not bind or only weakly bound to biotin–Aβ and biotin–hIAPP, IQIMIW and ITLFWG only bound to biotin–Aβ, and GTLFWG *vice versa*. These results indicate that upon immobilizing β-structure-forming SAPs (also including natively amyloid fragments ($Aβ_{27–32}$ and $hIAPP_{1–6}$)) onto the cellulose paper surface, they can still preserve their binding ability to recognize the Aβ and hIAPP *via* β-sheet interactions. Even for some SAPs that have no or weak β-sheet-forming property in bulk solution, surface immobilization could promote the β-structure formation and thus increase the binding probability to amyloid proteins to some extent. Visual inspection of chemiluminescence density appears to show the stronger binding recognition of biotin–Aβ by SAPs than biotin–hIAPP, presumably because Aβ peptides undergo faster aggregation kinetics (*e.g.*, the shorter lag phase) and have a higher β-sheet content (*e.g.*, a higher ThT intensity and CD peaks) than hIAPP peptides. This observation, at least in part, supports the significant role of β-structure interactions in SAP–Aβ/hIAPP recognition.

3.5 SAPs-coated SAP sensor to detect Aβ and hIAPP

To further confirm the above results and to quantitatively characterize the binding interaction of SAPs with Aβ or hIAPP, we presented an SAP-coated surface plasmon resonance (SPR) sensor for the detection of Aβ and hIAPP. As shown in Fig. 5a, carboxymethylated dextran (CBD) was first used to modify a gold SPR chip, because CBD is well-known to resist nonspecific protein adsorption[32] and also contains the carboxymethyl functional group (–CH_2–COOH) allowing for the effective and convenient immobilization of SAPs *via* simple 1-ethyl-3-(3-(dimethylamino)-propyl)-carbodiimide and *N*-hydroxysuccinimide (EDC/NHS) chemistry. Evidently, CBD-modified gold chips did not adsorb any Aβ and hIAPP (Fig. 5f). Then, three SAPs (**HP1**, **HP2**, **HP6** that consistently showed high and specific binding affinity to both Aβ and hIAPP in solution and at the surface), $Aβ_{27–32}$ and $hIAPP_{1–6}$ as a positive control, and PTRCGP as a negative control were selected to further conjugate onto the CBD-modified gold SPR chips *via* EDC/NHS reactions. Taking the detection of Aβ (Fig. 5b) and

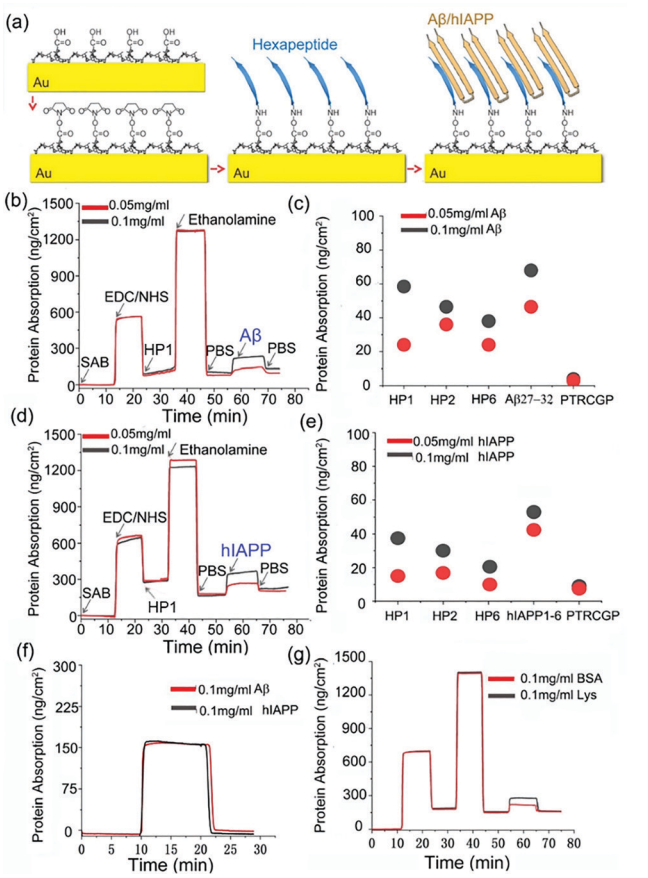

Fig. 5 SAP-coated SPR sensors for amyloid detection. (a) Schematic of a step-by-step construction of SAP-coated SPR sensors *via* sequential surface modification by carboxymethyl dextran and SAPs for the detection of Aβ or hIAPP. Typical SPR sensorgrams for measuring the adsorption amount of (b) Aβ, (d) hIAPP, and (g) BSA and Lys using (b, d, g) **HP1**-coated SPR sensors and (f) non-coated CBD SPR chips. The adsorption amount of (c) Aβ and (e) hIAPP on **HP1**-, **HP2**, **HP6**-coated SPR chips at different analyte concentrations, in comparison with the control surfaces coated by $Aβ_{27–32}$, $hIAPP_{1–6}$, and RTRCGP.

hIAPP (Fig. 5d) by **HP1**-coated, CBD-modified SPR chips as examples, the **HP1** sample was first flowed into SPR channels to conjugate onto a CBD-modified gold chip to form the **HP1**–CBD-modified chip, followed by ethanolamine washing to stop the EDC/NHS reactions, then applying the amyloid solution (Aβ or hIAPP) to flow through the **HP1**–CBD-coated chip for amyloid detection, finally using PBS to wash away unbound or weakly bound amyloid proteins. As a result, the total amount of adsorbed Aβ or hIAPP on any SAP-coated chip was determined by a wavelength shift between the two baselines before and after injecting amyloid solution. Our previous studies have shown that a 1 nm wavelength shift corresponds to ~15 ng mm^{-2} of adsorbed proteins.[33,34] On the basis of this model, Fig. 5c and e summarize the final amount of adsorbed Aβ and hIAPP on five different peptide-coated SPR chips. As positive controls, the $Aβ_{27–32}$-coated gold surface can detect 46.5 and 68.0 ng cm^{-2} of Aβ at 0.05 and 0.1 mg mL^{-1} concentrations, respectively, while the $hIAPP_{1–6}$-coated surface can detect 41.5 and 52.0 ng cm^{-2} of hIAPP at 0.05 and 0.1 mg mL^{-1} concentrations, respectively. In contrast, the PTRCGP-coated surface as a negative control only adsorbed very few Aβ (4.0 ng cm^{-2}) or hIAPP (6.0 ng cm^{-2}), almost independent of Aβ or hIAPP concentration. Such a large difference between two control experiments demonstrates the working feasibility and principle of this peptide-coated SPR sensor for the detection of Aβ and hIAPP in terms of β-sheet interactions between amyloid peptides and immobilized peptides.

Next, both Aβ and hIAPP amyloid solutions of two different concentrations (0.1 mg mL^{-1} to 0.05 mg mL^{-1}) were applied to the SAP-coated sensor chip to confirm the dual amyloid detection ability of SAPs. In general, all three **HP1**, **HP2**, and **HP6**-coated SPR sensors were able to detect both Aβ (Fig. 5c) and hIAPP (Fig. 5e). Among them, **HP1**-coated sensors (58.5 ng cm^{-2} of Aβ and 37.5 ng cm^{-2} of hIAPP) can detect more adsorbed Aβ and hIAPP at 0.1 mg mL^{-1} than **HP2**-coated sensors (46.5 ng cm^{-2} of Aβ and 30.1 ng cm^{-2} of hIAPP) and **HP6**-coated sensors (38.0 ng cm^{-2} of Aβ and 20.5 ng cm^{-2} of hIAPP) (Fig. 5, Fig. S7, S8, ESI†). While lowering the concentration of Aβ and hIAPP from 0.1 mg mL^{-1} to 0.05 mg mL^{-1} resulted in a decrease of the adsorbed amount of both Aβ and hIAPP (10.0–36.0 ng cm^{-2}), both amyloid proteins can still be detected by the three SAP-coated sensor chips, indicating a high detection sensitivity of SAP-coated SPR sensors. To prove that the SAP-coated SPR sensor can specifically detect amyloid peptides (Aβ and hIAPP), we also comparatively studied the ability of **HP1**-, **HP2**-, and **HP6**-coated SPR sensors to detect lysozyme and BSA proteins (0.1 mg mL^{-1}). The results showed that lysozyme and BSA cannot be detected by using the SAP-coated SPR chips (Fig. 5g and Fig. S9, ESI†), indicating that no specific binding occurs between lysozyme/BSA and SAP-coated sensors. Thus, both paper sensors and SPR sensors achieve consistent detection results. In a broader view, it is not surprising to observe the heterogenous recognition and interaction between heterogenous sequences (*i.e.* SAP *vs.* amyloids), and such heterogeneous-sequence interactions between dissimilar amyloid sequences (Aβ and α-synuclein,[35] between Aβ and tau,[36] between hIAPP and insulin[37] and even between bacterial curli and amyloid peptides of SEVI, Aβ, and hIAPP) were observed.[38] Thus, collective evidence from experiments and simulations confirm our "like-interacts-like" hypothesis that the β-structure in SAPs can serve as a general biorecognition motif to specifically interact with a similar structural motif of amyloid aggregates of different sequences *via* the homotypic β-sheet association.

We propose a "like-interacts-like" concept to *de novo* design a new class of SAPs, not derived from any amyloidogenic sequences, with built-in, multi-target, conformational-specific binding functions for the inhibition and detection of both Aβ and hIAPP in solution and on surfaces. From a structural viewpoint, this work provides a new conceptual strategy for the rational design of conformational-specific, sequence-independent peptides, capable of expanding its binding/detecting functions to different molecular-recognition applications of targeted drug therapy, biomarker detection, and disease diagnostics (*e.g.* cancers, COVID-19[39,40]). Based on the specific β-structure-rich feature of amyloids, current sensing probes are mostly protein-based molecules (*e.g.*, antibody, enzyme, protein receptor) or chemical-based molecules (*e.g.*, fluorescents, nanoparticles) with a single-target function for solely detecting specific amyloid fibrils.[2] In comparison to these common amyloid-recognition elements, small peptides can be used to develop highly sensitive, specific, and robust biosensors for the clinical diagnosis of disease-related biomarkers. Peptides are small in size which helps to decrease their susceptibility to proteases and non-specific binding/trapping of antigens, are often fabricated into label-free biosensors to reduce all unwanted side effects as introduced by tags and can be mass-produced through standard solid-phase synthesis at low cost. More importantly, different from other peptide-based amyloid probes whose sequences are exclusively derived from their parent amyloid proteins, our self-assembling peptides (SAPs) do not contain any amyloidogenic sequence, but they are able to self-assemble into β-sheet-rich structures conformationally similar to those in amyloid fibrils. Thus, our SAPs enabled to serve as general β-structure-recognition molecules by binding to similar β-structures of amyloid aggregates of different sequences, thus achieving both amyloid detection and amyloid inhibition functions.

4. Conclusion

In summary, we propose a "like-interacts-like" concept to *de novo* design a new class of SAPs, not derived from any amyloidogenic sequences, with built-in, multi-target, conformational-specific binding functions for the inhibition and detection of both Aβ and hIAPP in solution and on surfaces. The as-designed SAPs, particularly CILFWG, CTLWWG and GTVWWG, demonstrated not only their self-assembly ability to form β-structure-rich aggregates with non or less cell toxicity, but also their cross-interactions with both Aβ (associated with AD) and hIAPP (associated with T2D) to inhibit the aggregation of Aβ and hIAPP by 34–61% and reduce the amyloid-induced cell toxicity by 7.6–35.4%. Strong interactions of SAPs with amyloids allow them to be fabricated into the two types of paper sensors

and SPR sensors *via* different surface immobilization methods for realizing structural-specific detections of Aβ and hIAPP aggregates with high sensitivity. Conversely, VYIMIG and CTVFIG with a poor self-assembly property exhibited the weak amyloid inhibition, again confirming the important role of β-structure-rich conformation of SAPs in amyloid inhibition. The proposed design strategy allows us to greatly expand the peptide-based probes for amyloid detection beyond the few available today. For practical application of our amyloid probes and sensors, on-going efforts will focus on further optimizing both SAPs and sensor performance in order to achieve their uses in artificial or real cerebrospinal fluid/blood/serum samples for some practical applications.[41]

Author contributions

The manuscript was written through contributions of all authors. All authors have given approval to the final version of the manuscript. ‡These authors contributed equally.

Conflicts of interest

The authors declare no competing financial interest.

Acknowledgements

J. Z. thanks financial support from NSF (CBET-2107619), and partially from NSF (DMR-1806138) and Faculty Summer Fellowship at U. of Akron. We also trained three K12 students Keven Gong from Hudson Middle School, Bowen Zheng from Copley High School, and Alice Xu from Hudson High School *via* this project.

References

1 F. M. LaFerla, K. N. Green and S. Oddo, *Nat. Rev. Neurosci.*, 2007, **8**, 499–509.
2 Y. Zhang, B. Ren, D. Zhang, Y. Liu, M. Zhang, C. Zhao and J. Zheng, *J. Mater. Chem. B*, 2020, **8**, 6179–6196.
3 J. McLaurin, R. Cecal, M. E. Kierstead, X. Tian, A. L. Phinney, M. Manea, J. E. French, M. H. L. Lambermon, A. A. Darabie, M. E. Brown, C. Janus, M. A. Chishti, P. Horne, D. Westaway, P. E. Fraser, H. T. J. Mount, M. Przybylski and P. St. George-Hyslop, *Nat. Med.*, 2002, **8**, 1263–1269.
4 B. Solomon, R. Koppel, E. Hanan and T. Katzav, *Proc. Natl. Acad. Sci. U. S. A.*, 1996, **93**, 452–455.
5 C. Cabaleiro-Lago, I. Lynch, K. Dawson and S. Linse, *Langmuir*, 2009, **26**, 3453–3461.
6 E. N. Gurzov, B. Wang, E. H. Pilkington, P. Chen, A. Kakinen, W. J. Stanley, S. A. Litwak, E. G. Hanssen, T. P. Davis and F. Ding, *Small*, 2016, **12**, 1615–1626.
7 K. Debnath, S. Shekhar, V. Kumar, N. R. Jana and N. R. Jana, *ACS Appl. Mater. Interfaces*, 2016, **8**, 20309–20318.
8 J. Guo, J. Li, Y. Zhang, X. Jin, H. Liu and X. Yao, *PLoS One*, 2013, **8**, e65579.
9 Y. Xu, Y. Li, L. Wei, H. Liu, J. Qiu and L. Xiao, *Eng. Sci.*, 2019, **6**, 53–63.
10 B. Cheng, H. Gong, X. Li, Y. Sun, X. Zhang, H. Chen, X. Liu, L. Zheng and K. Huang, *Biochem. Biophys. Res. Commun.*, 2012, **419**, 495–499.
11 Y. Porat, A. Abramowitz and E. Gazit, *Chem. Biol. Drug Des.*, 2006, **67**, 27–37.
12 B. P. Ren, M. Z. Zhang, R. D. Hu, H. Chen, M. L. Wang, Y. F. Lin, Y. Sun, L. Y. Jia, G. Z. Liang and J. Zheng, *ACS Omega*, 2017, **2**, 243–250.
13 B. P. Ren, Y. L. Liu, Y. X. Zhang, M. Z. Zhang, Y. Sun, G. Z. Liang, J. X. Xu and J. Zheng, *J. Mater. Chem. B*, 2018, **6**, 56–67.
14 F. Pan, N. Zhou, J. Li, X. Du, L. Zhao, C. Wang, M. Zhang and X. Ai, *ES Food Agroforestry*, 2020, **2**, 58–69.
15 Y. Zhang, M. Zhang, Y. Liu, D. Zhang, Y. Tang, B. Ren and J. Zheng, *J. Mater. Chem. B*, 2021, **9**, 3300–3316.
16 Y. Zhang, Y. Tang, Y. Liu, D. Zhang and J. Zheng, *Adv. Funct. Mater.*, 2021, 2102978.
17 Y. Zhang, Y. Liu, Y. Tang, D. Zhang, H. He, J. Wu and J. Zheng, *Chem. Sci.*, 2021, **12**, 9124–9139.
18 E. A. Fradinger, B. H. Monien, B. Urbanc, A. Lomakin, M. Tan, H. Li, S. M. Spring, M. M. Condron, L. Cruz, C.-W. Xie, G. B. Benedek and G. Bitan, *Proc. Natl. Acad. Sci. U. S. A.*, 2008, **105**, 14175–14180.
19 K. L. Sciarretta, A. Boire, D. J. Gordon and S. C. Meredith, *Biochemistry*, 2006, **45**, 9485–9495.
20 C. W. Cairo, A. Strzelec, R. M. Murphy and L. L. Kiessling, *Biochemistry*, 2002, **41**, 8620–8629.
21 L. O. Tjernberg, J. Näslund, F. Lindqvist, J. Johansson, A. R. Karlström, J. Thyberg, L. Terenius and C. Nordstedt, *J. Biol. Chem.*, 1996, **271**, 8545–8548.
22 C. Soto, E. M. Sigurdsson, L. Morelli, R. A. Kumar, E. M. Castaño and B. Frangione, *Nat. Med.*, 1998, **4**, 822–826.
23 D. M. Walsh, M. Townsend, M. B. Podlisny, G. M. Shankar, J. V. Fadeeva, O. E. Agnaf, D. M. Hartley and D. J. Selkoe, *J. Neurosci.*, 2005, **25**, 2455–2462.
24 L. A. Scrocchi, Y. Chen, S. Waschuk, F. Wang, S. Cheung, A. A. Darabie, J. McLaurin and P. E. Fraser, *J. Mol. Biol.*, 2002, **318**, 697–706.
25 E. T. A. S. Jaikaran, C. E. Higham, L. C. Serpell, J. Zurdo, M. Gross, A. Clark and P. E. Fraser, *J. Mol. Biol.*, 2001, **308**, 515–525.
26 T. Takahashi and H. Mihara, *Acc. Chem. Res.*, 2008, **41**, 1309–1318.
27 B. M. Austen, K. E. Paleologou, S. A. E. Ali, M. M. Qureshi, D. Allsop and O. M. A. El-Agnaf, *Biochemistry*, 2008, **47**, 1984–1992.
28 Y. Qiao, M. Zhang, Y. Liang, G. Liang and J. Zheng, *Phys. Chem. Chem. Phys.*, 2017, **19**, 155–166.
29 Y. Tang, D. Zhang, Y. Zhang, Y. Liu, L. Cai, E. Plaster and J. Zheng, *J. Mater. Chem. B*, 2022, DOI: 10.1039/D1TB01942B.
30 H. Li, Y. Cao, X. Wu, Z. Ye and G. Li, *Talanta*, 2012, **93**, 358–363.
31 C. Chen, Y. Liu, J. Zhang, M. Zhang, J. Zheng, Y. Teng and G. Liang, *Chemom. Intell. Lab. Syst.*, 2015, **145**, 7–16.
32 L. Li, S. Chen, J. Zheng, B. D. Ratner and S. Jiang, *J. Phys. Chem. B*, 2005, **109**, 2934–2941.

33 C. Zhao, L. Li, Q. Wang, Q. Yu and J. Zheng, *Langmuir*, 2011, **27**, 4906–4913.
34 C. Zhao, L. Li and J. Zheng, *Langmuir*, 2010, **26**, 17375–17382.
35 P. K. Mandal, J. W. Pettegrew, E. Masliah, R. L. Hamilton and R. Mandal, *Neurochem. Res.*, 2006, **31**, 1153–1162.
36 I.-C. Stancu, B. Vasconcelos, D. Terwel and I. Dewachter, *Mol. Neurodegener.*, 2014, **9**, 1–14.
37 P. Liu, S. Zhang, M.-s. Chen, Q. Liu, C. Wang, C. Wang, Y.-M. Li, F. Besenbacher and M. Dong, *Chem. Commun.*, 2012, **48**, 191–193.
38 K. Hartman, J. R. Brender, K. Monde, A. Ono, M. L. Evans, N. Popovych, M. R. Chapman and A. Ramamoorthy, *PeerJ*, 2013, **1**, e5.
39 V. S. Shaikh, Y. I. Shaikh and K. Ahmed, *Eng. Sci.*, 2020, **12**, 113–116.
40 P.-y. Zhu, X. Bian, Y. Yang, Y. Fu, N. Wu, D.-h. Yu, L.-l. Liu, T.-l. Xing, X.-m. Zhang and Z. Na, *ES Food Agroforestry*, 2021, **5**, 4–13.
41 H. Hampel, S. E. O'Bryant, J. L. Molinuevo, H. Zetterberg, C. L. Masters, S. Lista, S. J. Kiddle, R. Batrla and K. Blennow, *Nat. Rev. Neurol.*, 2018, **14**, 639–652.

